MATHEMATICAL MODEL OF MOVING COKE BED FOR REDUCTION AND MELTING OF OXIDIZED IRON-SCRAP

Xinghe Zhang, Hiroshi Nogami, Reijiro Takahashi, Jun-ichiro Yagi

Institute for advanced Materials Processing, Tohoku University
2-1-1 Katahira, Aoba-ku, Sendai, 980-8577, JAPAN
Tel: +81-22-217-5174, Fax: +81-22-217-5211
E-mail: zhangxh@iamp.tohoku.ac.jp

ABSTRACT

The reduction and melting of oxidized iron-scrap briquettes containing coke breeze in a moving bed reactor has been proposed from the viewpoints of energy saving, recycling and environmental protection. The aim of this study is to investigate the effect of the briquette on operation of the reduction-melting furnace. For this purpose, a total mathematical model of the reduction-melting furnace has been developed based on the rates of briquette reduction and solid iron carburization and wetted area in a trickle bed.

The numerical simulation of the reduction-melting furnace described three-phase flow phenomena with chemical reactions and phase changes; specifically, the distributions of temperature, gas concentration, reduction degree and carburization degree in the furnace were calculated. The simulation results under different operating conditions showed that stable operation is obtained with blowing of preheated air at 673K or with 8% oxygen enrichment to air and with coke ratio fixed at 530 kg/thm.

1. INTRODUCTION

Briquettes of oxidized iron-scrap containing coke breeze are attracting much attention as a new raw material for ironmaking. It offers two benefits; enhancing the reduction of iron oxide and decreasing the melting temperature of burden due to carburization of iron. However, the effect of the briquette, properties and their performance in a moving coke-bed reactor is not well understood. This paper, therefore, deals with a mathematical model of a moving bed reactor for melting scrap, where the effect of the briquette containing coke breeze is assessed. The briquette and coke are charged into the furnace (see **Figure 1**), in which three-phase flow phenomena exists, together with phase changes and several major reactions such as combustion, reduction and carburization. The briquette moves down slowly, starts melting in a cohesive zone and trickles in the form of hot metal and molten slag in the lower part of the furnace. In contrast, cold air blasted through tuyeres flows up through packed materials. For the simulation of this reactor, three key parameters must be known; the rates of reduction and carburization, and wetted area. These were experimentally evaluated before the development of the mathematical model. Numerical simulation was finally carried out for analyzing the effect of the briquette containing coke breeze on reduction degree and temperature distributions within the reactor.
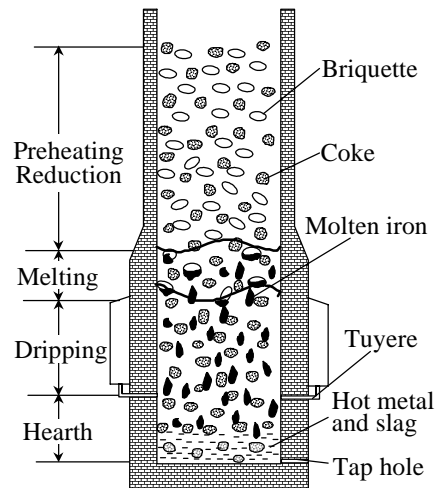

Figure 1: Schematic diagram of the reduction-melting furnace.

2. MATHEMATICAL MODEL

2.1 Governing Equations

In order to estimate the effectiveness of different briquettes (e.g. carbon content), a mathematical model, which simulates all phenomena of heat transfer, fluid flow and chemical reactions, is developed. The mathematical model consists of equations for conservation of mass, momentum, thermal energy and rate equations of heat exchange, chemical reactions and scrap melting. The methodology for mathematical modeling of multiphase flows has been described in previous papers (Yagi et. al., 1992a, 1992b and 1994). Based on these

investigations, transport phenomena can be described by the following general equation with several assumptions, i.e. steady state continuous flow, axisymmetry and no temperature gradient within packed materials.

$$\frac{\partial\,(\varepsilon_i\rho_i u_i\phi_i)}{\partial\,x}+\frac{1}{r}\frac{\partial\,(r\varepsilon_i\rho_i v_i\phi_i)}{\partial\,r}=\frac{\partial}{\partial\,x}(\varepsilon_i\Gamma_{\phi i}\frac{\partial\phi_i}{\partial\,x})+\frac{1}{r}\frac{\partial}{\partial\,r}(r\varepsilon_i\Gamma_{\phi i}\frac{\partial\phi_i}{\partial\,r})+S_{\phi i} \tag{1}$$

The dependent variable ϕ_i, diffusive transport coefficient Γ_{ϕ_i} and source term S_{ϕ_i} are described in **Table 1**. The source term includes interaction forces and gravity for momentum transfer, melting rate for mass transfer and heat exchange, reaction heat and melting heat for thermal energy transfer.

Gravitational flow of packed particles was described by the kinematic model (Nedderman and Tuzun, 1979), in which the horizontal (radial) velocity is proportional to the vertical velocity gradient in the horizontal direction ($v_s=-B(\partial\,u_s/\partial\,r)$). The value of B, the kinematic constant, is an empirical coefficient (is set equal to) 2.5 times the particle diameter.

Table 1 Dependent variable, diffusive transport coefficient and source term.

i	ϕ_i	Γ_{ϕ_i}	S_{ϕ_i}
g	1	0	S_{sg}
g	u_g	μ_g	$-\varepsilon_g\frac{\partial P_g}{\partial x}-F_{x,gs}-F_{x,gl}$
g	v_g	μ_g	$-\varepsilon_g\frac{\partial P_g}{\partial r}-F_{r,gs}-F_{r,gl}-\varepsilon_g\mu_g\frac{v_g}{r^2}$
g	h_g	λ_g/Cp_g	$\sum\limits_{i\neq g}a_{gi}h_{gi}(T_g-T_i)+\sum\limits_{k}\eta_{gk}(-\Delta H_k)R_k+\Delta H_{sg}^c$
g	m_n	$\rho_g D_g$	$\sum\limits_{k}\nu_{nk}R_k$
s	1	0	$-R_m-S_{sg}$
s	h_s	λ_s/Cp_s	$\sum\limits_{i\neq s}a_{si}h_{si}(T_s-T_i)+\sum\limits_{k}\eta_{sk}(-\Delta H_k)R_k$ $-\Delta H_{sg}^c-\Delta H_{sl}^c$
s	m_{Fe}	0	$-R_m$
l	1	0	R_m
l	u_l	μ_l	$-\varepsilon_l\rho_l g+F_{x,gl}-F_{x,ls}$
l	v_l	μ_l	$F_{r,gl}-F_{r,ls}-\varepsilon_l\mu_l\frac{v_l}{r^2}$
l	h_l	λ_l/Cp_l	$\sum\limits_{i\neq l}a_{li}h_{li}(T_l-T_i)+\Delta H_{sl}^c$

By substituting this relationship into the continuity equation for packed bed of particles, an equation is derived which is similar to the diffusion equation for the vertical velocity component:

$$\frac{\partial\,u_s}{\partial\,x}=\frac{1}{r}\frac{\partial}{\partial\,r}\left(rB\frac{\partial\,u_s}{\partial\,r}\right)-R_m-S_{sg} \tag{2}$$

Here, R_m is melting rate and is given by the rate of heat transfer to particles at the melting temperature.

Each conservation equation was discretized over the control volume (Patankar, 1980) and numerically solved with a convergence criteria of less 0.1 % of fractional residuals under the boundary conditions. Temperature dependence of all properties such as specific heat was taken into consideration in the computation.

2.2 Major Reactions

The various reactions considered in the mathematical model are shown in **Table 2**. For convenience, iron melting is also shown, though a phase change is not a chemical reaction. The rate of each reaction was incorporated as follows.

Table 2 Reactions in the reduction-melting furnace.

	Reaction	No.
Combustion and gasification of coke	$C + 1/2\ O_2 = CO$	1
	$C + O_2 = CO_2$	2
	$C + CO_2 = 2CO$	3
	$C + H_2O = CO + H_2$	4
Gaseous	$CO + 1/2\ O_2 = CO_2$	5
	$CO + H_2O = CO_2 + H_2$	6
	$H_2 + 1/2\ O_2 = H_2O$	7
Reduction	$Fe_nO_m + x\ C = n\ Fe + (2x\text{-}m)\ CO + (m\text{-}x)\ CO_2$	8
Carburization	$2CO = C_{(in\ Fe)} + CO_2$	9

2.2.1 Reactions of Coke and Gaseous

In the reactions of coke combustion and coke gasification, the total reaction rates, including chemical reaction and gas laminar film diffusion, were applied (Muchi et. al., 1966, Field et. al., 1967, Heynert et. al., 1959). Here, the reaction rate of complete combustion of C and O_2 was evaluated using the ratio between CO_2 and CO (Arthur, 1951).

$$R_k = \frac{a_c}{k_{fn}^{-1} + k_{ck}^{-1}} \frac{12\rho_g\varepsilon_g}{M_n} \tag{3}$$

$$k = 1,3,4 \quad n = 1,2,3$$
$$R_2: \quad C_4 / C_2 = 2500\exp(-6240 / T_s) \tag{4}$$

In the combustion reaction of CO, the Howard's equation (1973) was employed.

$$R_5 = 3.64 \times 10^{-10}\varepsilon_g C_4 C_1^{0.5} C_3^{0.5}\exp(-15106 / T_g) \tag{5}$$

We assumed that the water gas shift reaction and combustion of H_2 were equilibrium reactions.

2.2.2 Reactions of Briquette

Two kinds of briquette having different amounts of coke breeze were used in the numerical simulation. These are described in **Table 3**.

Table 3 Chemical composition of briquettes (mass%).

	T.Fe	M.Fe	Fe^{2+}	Fe^{3+}	O	C	C/O
B1	70.0	17.1	43.5	9.4	16.4	7.4	0.60
B2	67.0	17.7	42.3	7.0	15.1	11.2	0.99

C/O: Molar ratio of carbon and oxygen

Reaction rates for the reduction of iron oxide, the gasification of coke and the thermal decomposition of the binder in the oxidized iron-scrap briquette containing coke breeze were utilized. The reaction of a single briquette was studied experimentally by measuring changes of weight and gas volume at fixed temperature in a nitrogen atmosphere (Zhang et. al., 1995). The result was that reaction of the briquette is coincident with reactions of gasification of coke by CO_2 gas and reduction of iron oxide by CO gas. The reduction of iron oxide is in an equilibrium step and the gasification reaction is a rate-limiting step. It was, therefore,

concluded that the reduction rate of iron oxide is evaluated from the gasification rate shown below.

$$R_8 = k_8 m_{bc} \rho_b \varepsilon_b \tag{6}$$

For B1 briquette: $f_c^* = 1 - \exp(6.91 - 0.00568 T_s)$

$$k_8 = \begin{cases} 89.12 \exp\left(-138 \times 10^3 / RT_s\right) & (f_c \leq f_c^*) \\ 3.633 \exp\left(-116 \times 10^3 / RT_s\right) & (f_c > f_c^*) \end{cases}$$

For B2 briquette: $f_c^* = 1 - \exp(8.18 - 0.00675 T_s)$

$$k_8 = \begin{cases} 27.94 \exp\left(-123 \times 10^3 / RT_s\right) & (f_c \leq f_c^*) \\ 0.214 \exp\left(6.8 \times 10^3 / RT_s\right) & (f_c > f_c^*) \end{cases}$$

2.2.3 Carburization Rate

The carburization rate of solid iron by CO was obtained by thermo-gravimetrical analysis. The diffusion coefficient of carbon in solid iron was also obtained from the carbon content distribution in solid iron by EPMA analysis (Zhang et. al., 1997).

The carburization mechanism can be described as a two step process of surface carburization and diffusion of carbon into solid iron. The surface carburization reaction proceeds via two elemental reactions, as described below;

$$CO = O_{(ads)} + C_{(in\ Fe)}$$

$$O_{(ads)} + CO = CO_2$$

Here, dissociation of CO is in equilibrium and elimination of O adsorbed is rate-determining step. As a result, the reaction rate can be expressed below.

$$R_9 = k_9 \frac{K_9 p_{CO}^2}{K_9 p_{CO} + a_C} - k_9' \frac{a_C p_{CO_2}}{K_9 p_{CO} + a_C} \tag{7}$$

$$K_9 = 5.34 \times 10^{-13} \exp(168.8 \times 10^3 / RT)$$
$$k_9 = 1.61 \times 10^{-8} \exp(42.1 \times 10^3 / RT)$$
$$k_9' = 3.31 \times 10^6 \exp(41.6 \times 10^3 / RT)$$

2.2.4 Iron Melting Rate

The iron melting rate was calculated using equation (8) which was based on the assumption of the heat transfer being rate-limiting.

$$R_m = a_{gs} h_{gs} (T_g - T_m) / \Delta H_m \tag{8}$$

The melting point, T_m, was regarded as the surface melting temperature of iron. It was measured using a hot-stage microscope.

2.3 Parameter Evaluation

Before carrying out a numerical analysis using the mathematical model, unknown

parameters, such as contact area, exchange of momentum and heat transfer between heterogeneous phases, must be formulated.

2.3.1 Contact Area between Heterogeneous Phase

Obviously, liquid generation decreases both voidage and the contact area between gas and solid in the reduction-melting furnace. We assumed in this mathematical model that the dynamic hold-up of the liquid was assumed to be volumetric fraction of the liquid.

Equation (9) can be derived when occupied ratios of the three-phase (gas, solid and liquid) are expressed by their volume fraction ε_l, respectively.

$$\varepsilon_g + \varepsilon_s + \varepsilon_l \quad 1 \tag{9}$$

a_{gl} is the contact area between gas and liquid obtained by using Mada's equation (Mada, 1963), and a_{ls} the contact area between liquid and solid obtained by using Niu's equation (Niu et. al., 1996), which is the equation modified from Onda's equation (Onda et. al., 1967). a_{gs} is the contact area between gas and solid calculated as the difference in surface area of solid and contact area between liquid and solid. They can be expressed as following equations.

$$a_{gl} = 0.34 Fr_{ls}^{-1/2} We_{ls}^{2/3}/d_s \tag{10}$$

$$a_{ls} = \frac{6\varepsilon_s}{d_s} \{0.4(Re_{ls}/\varepsilon_s)^{0.218} We_{ls}^{00428} Fr_{ls}^{-0.0238} Nc^{-0.0235}\} \tag{11}$$

$$a_{gs} = 6\varepsilon_s/d_s - a_{ls} \tag{12}$$

2.3.2 Exchange of the Momentum

The interaction force between gas and solid was evaluated using Ergun's equation developed by considering the liquid-gas interaction. It is described by equation (13).

$$\vec{F}_{gs} = \left\{ \frac{150\mu_g a_s a_{gs}}{36(1-\varepsilon_s)} + \frac{1.75\rho_g a_{gs}}{6} |\vec{v}_g - \vec{v}_s| \right\} (\vec{v}_g - \vec{v}_s) \tag{13}$$

The interaction force between dripping liquid and rising gas through pore space in the packed bed was evaluated using Fanning's equation. This was developed by considering both the flows of gas and liquid in the packed bed and the contact area between gas and liquid. It is represented as equation (14).

$$\vec{F}_{gl} = \frac{a_{gl}}{a_{gl} + a_{sl}} \frac{3C_D \rho_g \varepsilon_l}{4d_l} |\vec{v}_g - \vec{v}_l|(\vec{v}_g - \vec{v}_l) \tag{14}$$

The interaction force between liquid and solid in the reduction-melting furnace was evaluated by the Kozeny-Carman equation developed using the contact area between liquid and solid. It is given as equation (15).

$$\vec{F}_{ls} = \frac{180\mu_l a_s a_{sl}}{36(1-\varepsilon_s)}(\vec{v}_l - \vec{v}_s) \tag{15}$$

2.3.3 Heat Transfer

The heat transfer coefficients between gas and solid and between gas and liquid represented as equation (16, 17) were evaluated using the Ranz-Marshall equation as modified by Akiyama et. al. (1990). The heat transfer coefficient between liquid and solids was evaluated by the equation (18), which is for forced convection heat transfer proposed by Pohlhausen (1921).

$$h_{gs} = (2.0+0.39Re_{gs}^{1/2}Pr_g^{1/3})\lambda_g/d_s \tag{16}$$

$$h_{gl} = (2.0+0.39Re_{gl}^{1/2}Pr_g^{1/3})\,\lambda_g/d_l \tag{17}$$

$$h_{ls} = (0.664Re_{ls}^{1/2}Pr_l^{1/3})\,\lambda_l/d_s \tag{18}$$

2.4 Experimental Verification

Before numerical simulations of the moving bed reactor was conducted, the mathematical model, together with rate parameters summarized above were experimentally verified using a laboratory-scale combustion furnace of a coke bed. **Figure 2** shows the comparison between observed and calculated distributions of temperature and gas composition within the furnace. The good agreement provides support for the underlying assumptions made in the model.

3. MATHEMATICAL SIMULATION

3.1 Simulating Conditions

3.1.1 Size of the Furnace

The reduction-melting furnace was a cylindrical vessel of 1 m inner diameter and 4.5 m effective height. The distance from the tuyere level to the molten iron surface was assumed as 400mm. The tuyere opening was 10 % of the
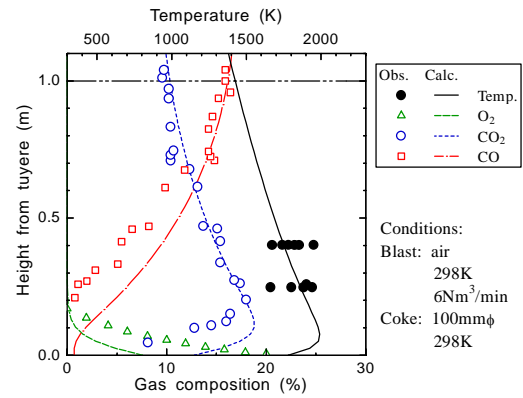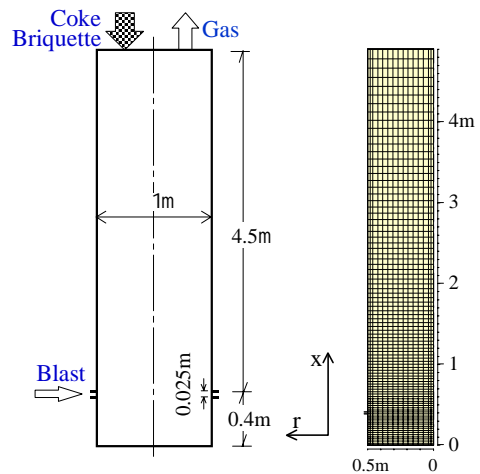
Figure 2 Comparison between calculated and measured longitudinal distributions of gas composition and

Figure 3 Size and grid arrangement for reduction-melting furnace.

cross-sectional area of furnace, with a slit width of 25 mm.

Since the furnace was axisymmetrical, the region for numerical analysis was decided as the half of the furnace. The flow domain was represented by a 90 by 15 grid, with finer resolution close to the tuyere.

3.1.2 Boundary Conditions

The boundary conditions are given as follows: no flux condition on center axis, zero velocity on the bottom of the furnace, slip condition on the wall and free boundary at the top. For the wall and the bottom of the furnace, the heat loss was also considered.

Regarding the gas phase, the flow rate, the composition and the temperature of the inlet gas were specified as constant values and the pressure of outlet gas was specified as an atmosphere at the furnace top. Regarding the solid phase, burden materials are continuously supplied at the furnace top, and the temperature and the coke ratio were fixed as constant values. Regarding the liquid phase, it is formed in the melting zone and continuously discharged from the furnace bottom.

3.1.3 Operating Conditions

The temperature and physical properties of charged burden materials for the numerical simulation of briquette melting process are given in **Table 4**.

Table 4 Operating conditions.

Material	Temp. (K)	Diameter (mm)	Porosity (-)	Density (kg/m^3)
Coke	298	50	0.52	1000
Briquette	298	35	0.48	3280

3.2 Results and Discussion

3.2.1 Reduction Degree of Briquette

Figure 4 shows the distributions of reduction degree of the briquettes, B1 and B2 under the condition of blowing preheated air at 673K. Significant differences in the results showed that the final reduction degree for the operation with briquette B2 was 30% higher than that with briquette B1. The high reduction degree of briquette B2 was caused by a high coke breeze content in the briquette. This clearly demonstrated the enhancement in reduction
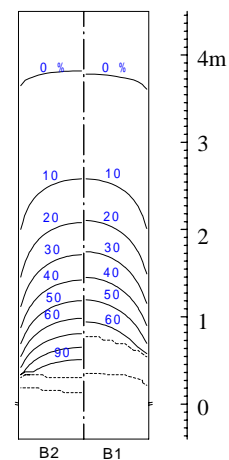
Figure 4 Computed distributions of reduction degree of briquette B1 and briquette B2.

rate of briquette with increasing carbon content.

3.2.2 Condition in Stable Operation

The briquette reduction-melting process was analyzed numerically by changing the air preheating temperature (313 ~ 873 K) and oxygen enrichment (0 ~ 14%), when charging briquette B2 and keeping coke ratio at 530 kg/thm. According to the numerical results, the briquette was not well melted due to the shortage of high temperature heat in the lower part of the furnace when the blast is not preheated to over 600K, or the oxygen enrichment is below 6% in the case of an ambient temperature blast.

Figure 5 shows numerical simulations of temperature distributions of gas, solid and liquid in the reduction-melting furnace when charging briquette B2 and keeping coke ratio fixed at 530 kg/thm. Case (a) is with air preheated at 673K but no oxygen enrichment, and Case (b) is with 8% oxygen enrichment to air with out preheating.

(a) Hot air blast (673K)   (b) Oxygen-enriched air blast (8%O₂)
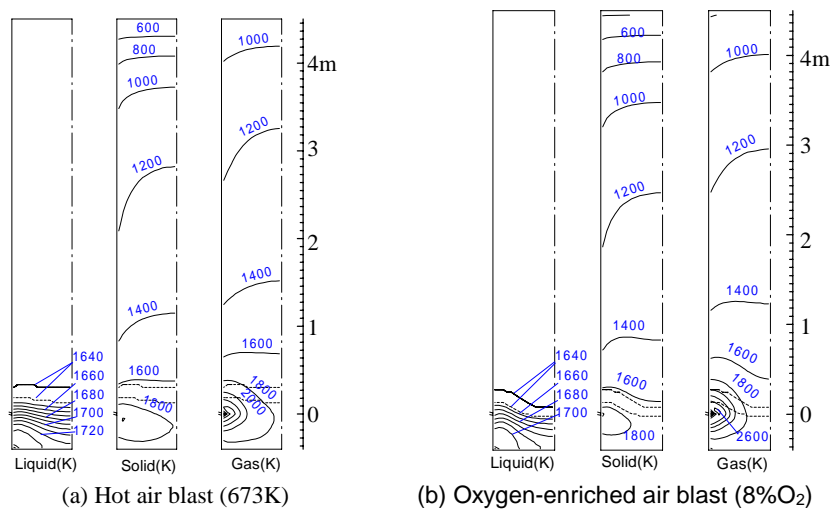
Figure 5 Computed isothermal lines of liquid, solid and gas for charging briquette B2.

In case (a), gas temperature rose to 2400K around the tuyere due to coke combustion, and then decreased to 860K at the outlet of the furnace. The charged briquette was heated up while descending and a melting zone appeared in the lower part of the furnace. The molten iron from the melting zone was heated to 1730K by gas and coke. Temperatures of gas and solid phases showed strong radial distribution in the upper part of the melting zone due to heat loss from the wall.

In case (b), the gas temperature rose to 2600K around the tuyere. This maximum temperature was 200K higher than that in case (a), however, the high-temperature region was narrower. Therefore, the melting zone was no longer horizontal, being higher near the wall and lower at the center of the furnace. The temperature of molten iron was 30K lower than

that in case (a), though the gas temperature was higher.

4. CONCLUSION

Oxidized iron-scrap briquettes containing coke breeze were investigated for use as a new raw material for hot metal production. A total mathematical model of the reduction-melting furnace has been developed based on the theory of mass and heat transport phenomena, and reaction kinetics. The model was experimentally verified by using a laboratory-scale furnace consisting of a coke bed.

The numerical simulation describes three-phase flow phenomena, with chemical reactions and phase changes. The distributions of temperature, gas concentration, reduction degree and carburization degree in the reduction-melting furnace are calculated. The reduction degree distribution showed that the charging of briquette B2 was better than the charging of briquette B1. This was due to a higher content of coke breeze in briquette B2 than briquette B1. Simulation results for different operating conditions showed that stable melting of the oxidized iron-scrap briquette was been obtained under preheated air blowing at 673K or with 8% oxygen enrichment to air blowing in the case of coke ratio fixed at 530 kg/thm.

NOMENCLATURE

a Area [m^2/m^3-bed] ΔH^c
C_D Drag coefficient [-]
C_p Specific heat [J/kg K]
d Mean particle diameter [m]
f_c Gasification degree of a briquette [-]
$\bar{F}$ Volumetric momentum flux [N/m^3]
Fr Froude number ($= a_j G_i^2 / \rho_i^2 g$) [-]
$F_{r,ij}$ Radial interaction force between phases i and j [N/m^3]
$F_{x,ij}$ Vertical interaction force between phases i and j [N/m^3]
g Gravitational force [m/s^2]
G Mass flow rate [$kg/m^2 s$]
ΔH^c Enthalpy transfer [W/ m^3-bed]
ΔH_k Enthalpy change [J/ kg]
h Enthalpy [J/kg]
h_{ij} Heat transfer coefficient between phases i and j [$W/m^2 K$]
k_{ck} Surface reaction rate constant (k=1-4) [m/s]
k_{fn} Mass transfer rate of n component [m/s]
k_k Reaction rate constant for reaction k [1/s]
m Fractional mass [-]
M Molecular weight [kg/kmol]
N_c Dimensionless surface tension, N_c=(1+cosθ) [-]

P Pressure [Pa]
Pr Prandtl number [-]
R Gas constant [J/mol K]
r Radial distance [m]
Re Reynolds number ($= G_i d_j / \mu_i$) [-]
R_k Reaction rate of k-th reaction [kg/s m^3-bed]
R_m Melting rate [kg/s m^3-bed]
S Source term [(kg m/s, J, kg)/ s m^3-bed]
S_{sg} Mass transfer from solid to gas [kg/s m^3-bed]
T Temperature [K]
u Vertical velocity [m/s]
v Radial velocity [m/s]
$\vec{v}$ Velocity vector [m/s]
We Weber number ($= G_i^2 / a_j \rho_i \sigma_i$) [-]
x Vertical distance [m]

Superscript
$*$ Critical

Subscript
b Briquette
bb Binder in briquette
bc Carbon in briquette
c Coke
g Gas

i,j	Phase	η	Distribution ratio of reaction heat [-]
k	Reaction number	λ	Thermal conductivity [W/m K]
l	Liquid	μ	Viscosity [Pa s]
n	Gas species (O_2, CO_2, H_2O, CO, H_2, N_2)	ν	Stoichiometric coefficient [-]
	Greek	θ	Contacting angle [degree]
ϕ	Dependent variable [(kg m/s, J, kg)/kg]	ρ	Density [kg/m^3]
Γ	Diffusive transport coefficient [kg/m s]	σ	Surface tension [N/m]
ε	Volumetric fraction [m^3/m^3-bed]		

REFERENCE

Akiyama T., Takahashi R. and Yagi J., (1990), Tetsu-to-Hagane, **76**, 848 - 855.

Arthur J.A, Trans, (1951), Faraday Soc., **47**, 164.

Ergun S., (1952), Chem. Eng. Progr., **48**, 89 - 94.

Field M.A, Gill D.W., Morgan B.B. and Hawksley P.G.W., (1967), Combustion of Pulverized Coal, BCURA, Leatherhead, Cherey and Sons, Banbury, England.

Heynert G. and Willems J., (1959), Stahl u. Eisen, **79**, 1545 - 1554.

Howard J. B., Williams G. C. and Fine D. H., (1973), 14th Int. Symposium on Combustion, Pittsburgh, 975 - 986.

Mada J., Shinohara H. and Tsubahara M., (1963), Kagaku Kougaku, **27**, 978 - 982.

Muchi I., Yagi J., Tamura, K. and Moriyama A., (1966), J. Japan Inst. Metals (Japanese), **30**, 826- 31.

Nedderman R. and Tuzun U., (1979), Powder Tech., **22**, 234 - 238.

Niu M., Akiyama T., Takahashi R. and Yagi J., (1996), AIChE J., **42**, 1181 - 1186.

Niu M., Akiyama T., Takahashi R. and Yagi J., (1996), Tetsu-to-Hagane, **82**, 647 - 652.

Onda K., Takeuchi H. and Koyama N., (1967), J. Chem. Eng.,(Japanese), **31**,.126 - 133.

Patankar S.V., (1980), Numerical Heat Transfer and Fluid Flow [Hemisphere Pub. Corp.].

Pohlhausen, E., (1921), Z. Angew. Math & Mech., **1**, 115 - 121.

Yagi J., Akiyama T. and Wang J., (1992a), Chemical Engineering, (Japanese), **37**, 207 - 216.

Yagi J., Akiyama T. and Nogami H., (1992b), Chemical Engineering, (Japanese), **37**, 769 - 779.

Yagi J. and Nogami H., (1994), Proc.4th Asian Conf. on Fluidized-Bed & Three-Phase Reactors (edited by Yoshida K. and Morooka S.), 235 - 240, Fukuoka, Japan.

Zhang X., Takahashi R. and Yagi J., (1995), Tetsu-to-Hagane, **81**, 1043 - 1048.

Zhang X., Takahashi R. and Yagi J., (1997), Tetsu-to-Hagane, **83**, 299 - 304.